

Structural changes in metastable epitaxial Co/Mn superlattices

K. Ounadjela, P. Vennegues, Y. Henry, A. Michel, V. Pierron-Bohnes, and J. Arabski

*Institut de Physique et Chimie des Matériaux de Strasbourg, Groupe d'Etudes des Matériaux Métalliques,
4 rue Blaise Pascal, 67070 Strasbourg, France*

(Received 2 August 1993)

Single crystalline epitaxial Co/Mn superlattices have been grown on a (0001) Ru buffer layer onto mica substrates. The evaporation of a seed layer of 6 Å Mn is necessary to obtain a high-quality epitaxial growth. Reflection high-energy electron diffraction, x-ray diffraction, and ferromagnetic resonance experiments clearly show a modification of the Mn structure, when the thickness of the Mn interlayer increases. The Mn structure switches from a compact phase close to the fcc Mn- γ for few atomic planes, to a less compact one, probably a Laves phase (MgCu₂) which resembles Mn- α , for larger thicknesses of Mn. This behavior induces a variation of the structure in the Co layers where the stacking changes from fcc to hcp. Up to six Mn atomic planes, the Mn layers being highly strained, the stabilization of the fcc Mn and Co metastable structures occurs via elastic and chemical interactions. For larger Mn thicknesses, there is a trade-off between reduced strains and a higher density of epitaxial dislocations, leading to a lower coherence between the Mn and Co layers. This leads the Mn and Co to approach their bulk structure, Mn- α and hcp, respectively. However, the chemical interactions between Co and Mn favor the fcc Co stacking and consequently create a large density of stacking faults in the hcp Co, even when the Mn is no longer close packed.

I. INTRODUCTION

Epitaxial thin-film structures offer unique opportunities for exploring the relationship between structure and magnetism. On an atomic scale, new phases [bcc Ni (Ref. 1) or Co (Ref. 2), hcp Fe (Ref. 3), for example] can be stabilized in thin films on suitable growth templates by molecular-beam epitaxy. *Ab initio* calculations have predicted various magnetic properties for such metastable structures including dramatic variations in magnetic moments,^{4,5} ferro- or antiferromagnetic ordering for expanded lattice materials that are normally nonmagnetic,⁶ and unusual magnetic anisotropies in ultrathin films.⁷

The initial interest of our work is based upon the magnetic and structural behavior of Mn atoms in numerous metallic environments. Mn atoms can occupy a wide range of atomic volumes and be in a number of different structural configurations. They have four different structures when varying the temperature in the bulk state. The α and β phases are complex cubic structures with 58 and 20 atoms per unit cell, respectively, whereas the γ and δ phases are face-centered cubic and body-centered cubic with nearest-neighbor spacings of 2.73 and 2.67 Å, respectively.⁸

Total-energy calculations have been used to investigate the low-temperature volume dependence of the magnetic behavior for bcc (Refs. 5, 6, and 9) and fcc (Ref. 10) Mn, phases which occur naturally, but at temperatures well above reasonable magnetic ordering temperatures. At low temperatures, both phases are predicted to order magnetically if the lattice spacing exceeds some minimum value.

Because of its exotic structural and magnetic properties, Mn is an interesting candidate for thin-film growth, as it is expected to accept different local configurations. Up to now, there has been only limited information on

the structure of Mn films on metallic substrates. Previous studies of Mn overlayers on Ru(0001),¹¹ Pd(111),¹² Fe(001),¹³ and Ag(001) (Ref. 14) substrates have made great efforts to expand the Mn lattice to produce large magnetic moments approaching the Hund's-rule limit of $5\mu_B$. In the case of Mn on Co, the lattice mismatch depends on the crystallographic structure of Mn. There is a large atomic volume difference between Mn in its different phases, for example, in α -Mn (12.217 Å³/atom) (Ref. 8) and γ -Mn (14.40 Å³/atom) (Ref. 8) and the cobalt in the fcc structure (11.108 Å³/atom), making difficult a coherent epitaxial growth of Mn on (111) Co layers.

Recent theoretical studies have produced interesting predictions about the variation of the oscillating exchange coupling between two adjacent cobalt layers depending on the structural coherence of the epitaxial growth of the Co/Mn superstructure. Stoeffler *et al.*,¹⁵ doing *ab initio*, spin-polarized, electronic-structure calculations within the framework of the local-spin-density approximation, have calculated the exchange coupling of the hcp (0001) Co/Mn superlattices and determined the period of the oscillating behavior of the exchange coupling as a function of the Mn thickness. They found that this period varies from 2 to 3.5 monolayers just by contracting the structural lattice parameter of the Mn by about 3%. This strain of the structure is the origin of a loss of the antiferromagnetic order of Mn from one plane to the other along the stacking direction. Thus they attribute the variation of the period to the magnetism of the spacer. This result shows the importance of the structural study of the as-grown epitaxial Co/Mn superlattices, the determination of the structural lattice parameter of both Co and Mn sublayers, and the corresponding stackings.

In this paper we describe the structural study of epitaxially grown Co/Mn superlattices. It shows a phase

change of the Mn layers depending on their thickness, switching from a compact phase close to the Mn- γ for few atomic planes to a less compact one in terms of hard sphere stacking, presumably close to a Laves phase (MgCu₂) for larger thicknesses of Mn. This behavior induces a variation of the structure in the Co layers.

In Sec. II we present the growth method and describe the preparation of the systems. Section III is devoted to the reflection high-energy electron-diffraction (RHEED) analysis which gives information on the quality of the films and their structural characteristics. The x-ray experiments are described and analyzed in terms of structure and coherence in Sec. IV. We report in Sec. V the results of ferromagnetic resonance (FMR) experiments which provide information on the structural quality of the cobalt layers. In Sec. VI the results are summarized and discussed in terms of competition between elastic strains and chemical energies.

II. Mn/Co SUPERLATTICES PREPARATION

Epitaxial growth of Co/Mn superlattices was carried out in a RIBER *e*-beam evaporator system on mica substrates. The mica substrates were freshly cleaved before introduction in the UHV chamber and heated up *in situ* to 680°C in order to drive off impurities. Then a 150-Å epitaxial Ru buffer layer was grown at 680°C in order to provide a smooth and clean single-crystalline surface. We subsequently cooled the substrates down to -15°C; this temperature turned out to be a good compromise between high crystalline quality and reduced intermixing between sublayers. All superlattices were covered by a 40-Å (0001) Ru cap layer to inhibit the surface contamination.

Mn and Co layers were grown at a rate of 6 Å/min out of an electron-beam hearth, monitored by a quartz microbalance. The base pressure prior to film growth was approximately 5×10^{-11} Torr, while during the growth it was around 5×10^{-10} Torr or better. In order to favor the epitaxial growth of Co/Mn with an in-plane sixfold symmetry, we found that it was essential to begin the growth with a 6-Å Mn layer. No single-crystalline Co/Mn multilayer was obtained at this growth temperature in the absence of this seed layer. Despite the large difference between Co and Mn bulk atomic volumes (10–20%), the growth of Co/Mn superlattices on a hcp (0001) Ru buffer layer is epitaxial.

Two series of Co/Mn superlattices were grown with 12- and 24-Å Co layers, the Mn layer thicknesses ranging between 3.2 and 32 Å. In the following, we refer to the nomenclature $[\text{Co}_{t_{\text{Co}}}/\text{Mn}_{t_{\text{Mn}}}]_N$ superlattice, where t_{Co} and t_{Mn} indicate the thicknesses in Å of the Co and Mn sublayers and N the number of periods. This study was carried out by *in situ* RHEED with a beam energy of 20 keV, *ex situ* x-ray diffraction, and X-band FMR performed at room temperature.

III. RHEED ANALYSIS

The crystallographic structure and crystalline quality of the Co/Mn superlattices have been examined by *in situ*

reflection high-energy electron diffraction. This technique gives a direct indication on the dynamical growth process and allows the determination of the crystal surface structure. Moreover, the in-plane lattice parameter of the free surface can be determined quantitatively from the distance between the RHEED streaks. Finally, for certain conditions of surface roughness, RHEED provides significant information about the volume structure.

A. Qualitative aspects

The RHEED patterns obtained during the sample growth reveal well-defined and reproducible structures. The main features observed on the successive Ru, Mn, and Co layers are described and discussed below.

(i) Figures 1(a) and (a') show the RHEED patterns observed along the $(\bar{1}\bar{2}10)$ and $(10\bar{1}0)$ azimuths of the hcp (0001) Ru buffer layer. These figures, observed with a six-fold symmetry, are characteristic of a close-packed structure [hcp (0001) or fcc (111)]. The two-dimensional (2D)

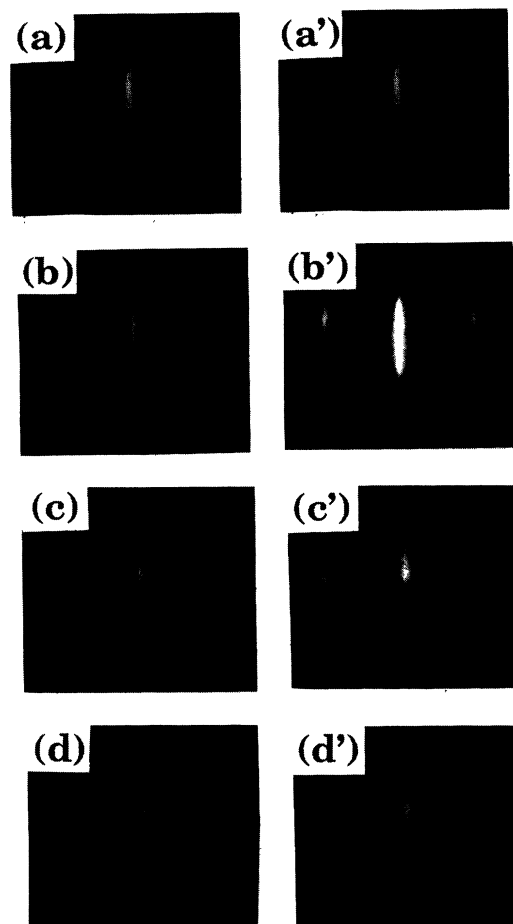


FIG. 1. RHEED patterns of $[\text{Co}_{24\text{Å}}/\text{Mn}_{24\text{Å}}]_{12}$ along the two characteristic azimuths [left $(\bar{1}\bar{2}10)$ and right $(10\bar{1}0)$] on (a),(a') Ru buffer, (b),(b') after 3 monolayers of Mn on the Ru buffer, (c),(c') after 3 monolayers of Mn on the first Co layer and (d),(d') after depositing the second Mn layer on top of the first Co layer.

character of the surface is evidenced by the presence of elongated and thin RHEED streaks. In addition, the (2×2) surface reconstruction is a strong indication of high crystalline quality. These patterns have been used for lattice spacing calibration, assuming that the Ru in-plane lattice parameter was the bulk one (2.71 Å). In the following, the $(\bar{1}210)$ and $(10\bar{1}0)$ azimuths will always refer to the Ru buffer.

(ii) Figures 1(b) and (b') show the RHEED patterns observed along the $(\bar{1}210)$ and $(10\bar{1}0)$ directions at the end of the Mn seed layer growth. The latter corresponds to the completion of 3 pseudomorphic monolayers epitaxially grown on the (0001) Ru buffer layer. Indeed, the patterns clearly show that the Mn seed layer replicates the orientation and lattice spacing of the Ru buffer layer. Except for the disappearance of the (2×2) surface reconstruction, we do not observe any significant change of the surface quality when Ru is covered by the seed layer. This initial layer is necessary to generate the following growth.

(iii) The growth of the Co overlayers onto the Mn layers always improves the RHEED pattern quality.¹⁶ Indeed, the streaks become more intense and thinner with marked decrease of spot intensity. This shows that the Co wets the Mn surface well and does not form small thick clumps. This indicates that Co tends to adopt a 2D growth mode. The Co growth behavior is significantly different from that of Mn, and the diffraction figures demonstrate that Co always grows in a close-packed structure even when the Mn underlayer is in a less compact structure as explained hereafter.

(iv) The RHEED patterns of the Mn overlayers deposited on Co layers consist of less intense and more diffused streaks [Figs. 1(c) and (c')] compared to those observed on the Co surface. This may be due to a slight misorientation of the grains over the Mn surface. With increasing Mn thicknesses, spots appear on the streaks, indicating that the incident electron beam transmits through blocks or islands nucleating on the flat surface. The blocks have a lateral size smaller than the electron-beam coherence length (few hundred angstroms). This shows a degradation of the surface flatness and suggests a three-dimensional growth mode of the Mn overlayers onto Co.

The beginning of each Mn sublayer deposition shows a surprising behavior. After the growth of about a quarter of Mn monolayer, two networks of equidistant streaks become visible and coexist along both $(\bar{1}210)$ and $(10\bar{1}0)$ azimuths [Figs. 1(c) and (c')], the appearing one corresponding to the diffraction of the growing Mn overlayer and the other to the cobalt underlayer. The streaks corresponding to Co keep the same position and width, their intensity merely decreases as the Mn layer gets thicker. They totally disappear after the growth of about 2 Mn monolayers. Simultaneously, the intensity of the streaks corresponding to the Mn progressively increases, whereas their position varies slightly. This result shows, on the one hand, that the cobalt is simply covered by the Mn with no change of its lattice parameter, on the other hand, that the free Mn top atomic planes grow incoherently onto the cobalt sublayer. Thus it suggests that the Co/Mn interface is bounded by misfit disloca-

tions. During this first stage of the Mn growth and up to 5 to 6 monolayers, the RHEED patterns retain the six-fold in-plane symmetry and the characteristic distance ratio between the streaks in both azimuths, corresponding to a compact Mn structure [fcc (111) or hcp (0001)]. Afterwards ($t_{\text{Mn}} > 12 \text{ \AA}$), additional streaks appear on the patterns observed along the $(10\bar{1}0)$ azimuth, while the $(\bar{1}210)$ azimuth patterns are unchanged [Figs. 1(d) and (d')], resulting in a commensurate 3×1 (or equivalently $[\sqrt{3} \times \sqrt{3}]r30^\circ$) structure. The intensity of the "fractional-order" streaks increases and becomes almost equal to that of the "integral-order" streaks after the deposition of 10 to 12 Mn monolayers. This is indicative of a high-stability bulk structure rather than of only a surface reconstruction and demonstrates the existence of a new Mn structure having a unit cell with the in-plane lattice constant $\sqrt{3}$ times larger than that of close-packed Mn, reoriented by 30° . This structural change, which occurs during the growth of Mn on cobalt, is observed periodically as every bilayer is grown during the whole deposition.

B. Quantitative aspects

Let us now consider the variation of the in-plane lattice parameter deduced from the RHEED patterns observed during the deposition of the $[\text{Co}_{24} \text{ \AA} / \text{Mn}_{24} \text{ \AA}]_{12}$ superlattice. This variation is shown in Fig. 2. The lattice parameter behavior seen in this sample is representative of that observed throughout the entire $[\text{Co}_{24} \text{ \AA} / \text{Mn}_{t_{\text{Mn}}}]_{12}$ series of samples when varying the Mn thickness. It should be borne in mind that the data in Fig. 2 represent the lattice parameter of any particular layer when that layer is the free surface layer: this parameter may subsequently vary by successive covering¹⁷ due to induced strain (see Sec. IV).

As shown in Fig. 2, the in-plane lattice parameter of the first Co monolayers grown on Mn appears quite expanded and relaxes toward the Co bulk value ($a_{\text{Co}} = 2.51 \text{ \AA}$) within 5–7 monolayers depending on the underlying Mn parameter ($a_{\text{Mn}} = 2.71 \text{ \AA}$ for samples with $t_{\text{Mn}} > 12 \text{ \AA}$ and $2.71 < a_{\text{Mn}} < 2.85 \text{ \AA}$ for samples with $t_{\text{Mn}} < 12 \text{ \AA}$). This suggests a semicoherent growth of the Co layers on Mn with a progressive decrease of the elastic expansive strains and increase of the dislocation density at the interface.

By contrast, the growth of the following Mn monolayers on Co appears to be incoherent since there is a discontinuity in the lattice parameter on deposition of the first Mn monolayer. Indeed, the latter has an in-plane lattice spacing of about 2.85 Å, which is 15% larger than that of the underlying Co layer.

The behavior of the Mn in-plane parameter for subsequent layers divides into two distinct regimes. Initially, the lattice parameter decreases progressively; afterwards, it reaches a plateau. The borderline between these two regimes coincides with the structure change which occurs after the growth of 5–6 Mn atomic planes. It is clear from the persistence of the characteristics of the RHEED patterns in the first regime that the structure of the 5–6

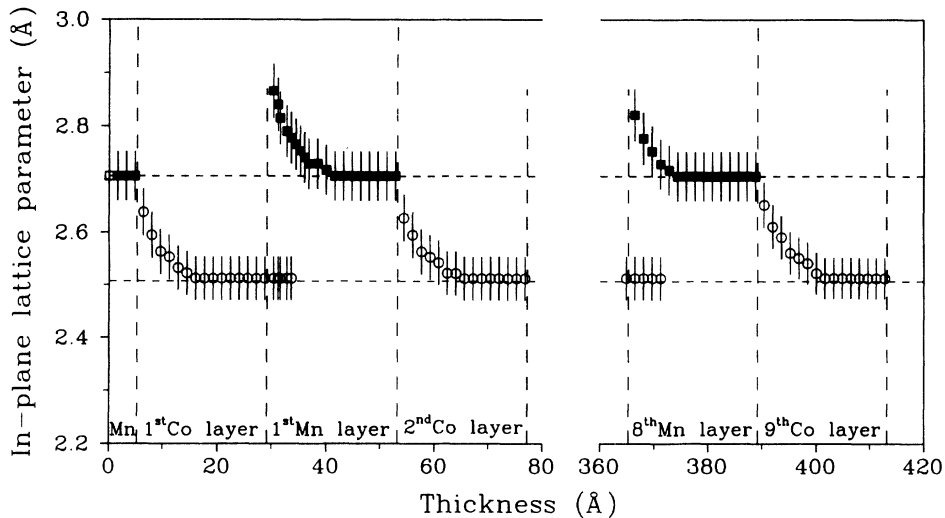


FIG. 2. Variation of the in-plane lattice parameter with the increasing thickness for the $[\text{Co}_{24} \text{ \AA} / \text{Mn}_{24} \text{ \AA}]_{12}$ superlattice measured during the film growth.

initial Mn monolayers is close packed. For bulk Mn, the only stable close-packed structure is the fcc γ -Mn phase, which is stable in the 1095–1134 °C temperature range and in which the nearest-neighbor distance is $a_{\gamma\text{-Mn}} = 2.73 \text{ \AA}$.⁸ If this material is quenched at room temperature (where it is metastable), the nearest-neighbor distance becomes even smaller [$a_{\gamma\text{-Mn}} = 2.67 \text{ \AA}$ (Ref. 8)]. This value is far from those obtained in the first regime where the in-plane nearest-neighbor distance varies from 2.85 to 2.71 Å.

As long as the Mn lattice parameter is concerned, a qualitative analysis of the results can be based on the following conjectures: (i) It seems likely that the structure of the first 5–6 monolayers grown on Co is similar to that of γ -Mn, but suffers a distortion corresponding to an expansion of the in-plane lattice parameter. The position of the free energy minimum is initially dominated by the surface energy term and corresponds, in a constant-volume hypothesis, to an expansion of the in-plane lattice spacing probably due to an out-of-plane compressive strain (evidenced by x-ray diffraction; see Sec. IV) originated by interactions with the Co underlayer. Such in-plane lattice expansion due to out-of-plane strains, which may be surprising, have already been observed in Ni/Mo superlattices,¹⁸ Pt on Fe(100),¹⁹ and even in complex structures such as high- T_c epitaxial superconductors.²⁰

(ii) As the Mn layer becomes thicker, the increasing ratio of volume to surface energy terms causes the lattice parameter to relax toward that of bulk quenched γ -Mn. However, this value is never reached because, at a thickness for which the in-plane lattice parameter is 2.71 Å, the structure change from the fcc to the new Mn phase interyenes and the distance between the RHEED streaks and the related lattice parameter remain constant, corresponding to those of the new phase.

The description of such a similar Mn phase has already been reported for Mn grown on (0001)Ru (Ref. 11) and (111) Pd (Ref. 12) in which a commensurate $[\sqrt{3} \times \sqrt{3} (r30^\circ)]$ structure in thin Mn layers has been observed. From the analysis of the RHEED patterns observed on Mn layers deposited on (0001) Ru, Heinrich

*et al.*¹¹ deduced models for the Mn structure which result in a more dense packing than that imposed by the Ru substrate. Indeed, they suggest that the tripling of the unit-cell area can be understood in terms of an increase of the Mn density in the ratio of 4 to 3 compared to the Ru substrate density. Given that, Mn atoms may have two different effective sizes, as, for example, in α -Mn, which result on a less compact structure in terms of hard sphere arrangement. Then three different structures are suggested for this new Mn phase, all of which are consistent with the tripling of the RHEED patterns. They are the CaCu_5 , MgZn_2 , and MgCu_2 structures. Among these, the hexagonal MgZn_2 and cubic MgCu_2 Laves phases seem more likely since both are based upon the hexatetrahedron, which is the basic building block of α -Mn.

In a forthcoming paper, Henry *et al.*,²¹ using 3D RHEED diffraction on the Mn layers deposited on Co, show that the phase change in Mn layers which occurs at 5–6 monolayers is not sharp and leads to the coexistence of crystal domains which have, respectively, the (111) MgCu_2 Laves-phase-type and (111) fcc structures. The amount of the MgCu_2 phase increases with Mn thickness at the expense of the fcc one. This tends to confirm the fact that, in the early stage of Mn growth, the close-packed Mn structure is fcc.

A 3D analysis, such as that reported by Henry *et al.*²¹ for the Mn surfaces, was not possible for the Co layers since the surface roughness was not sufficient to lead to an exploitable 3D diffraction. Hence a complete study of the cobalt structure was performed using x-ray diffraction and ferromagnetic resonance and is discussed in the next sections.

IV. X-RAY RESULTS

For the structural characterization of our superlattices, we used a high-resolution x-ray Philips diffractometer (HRXRD). A four-Ge(220)-crystal monochromator is introduced in the incident Cu radiation beam, providing a pure Cu $K\alpha_1$ parallel beam. The sample holder can be oriented following three perpendicular axes ω , R , and ϕ ,

which can be rotated by 170° , 360° , and 10° , respectively. The geometry of the diffractometer allows only experiments in reflection mode. All experiments were performed *ex situ* at room temperature. We carried out a complete study on the series of samples

$[\text{Co}_{24} \text{ \AA} / \text{Mn}_{t_{\text{Mn}}}]_{12}$ where t_{Mn} varies from 3.2 to 32 \AA. In order to obtain a relatively complete study of the reciprocal space of the Co/Mn superlattices, scans in three different geometries (Fig. 3) were carried out.

A. $\theta/2\theta$ scans

Reflectivity measurements can scan the Q_z reciprocal line perpendicular to the film plane [Fig. 3(a)]. We performed only high-angle scans around the first-order Bragg peak. The curvature of the mica (few tenths of a degree) and the presence of steps due to cleavage prohibit small-angle reflectivity studies. The high-angle scans analysis yields information on the structural coherence of the superlattice along the growth direction (L_1), on the average lattice spacing (D), and on the superlattice period ($t_{\text{Co}} + t_{\text{Mn}}$). D is deduced from the position of the main Bragg peak (SL_n), while the coherence length normal to the film surface is deduced from the full width at half maximum (FWHM) of SL_n and ($t_{\text{Co}} + t_{\text{Mn}}$) from the distances between the satellites. The presence of satellites is a direct evidence of the composition modulation.

For elements near in the periodic table such as Co and Mn ($\Delta Z = 2$), the atomic form-factor contrast is very weak. Using the Cu $K\alpha_1$ characteristic radiation, which is close to the Co K absorption edge, the contrast is still weaker than using other wavelengths. The presence of satellite peaks down to a 4.8 \AA thickness of Mn as shown in Fig. 4 demonstrates the high quality of the composition modulation. To increase the atomic form-factor contrast, it is possible to work with a radiation at an energy close to the absorption edge of the Mn. Indeed, anomalous $\theta/2\theta$ spectra on a $[\text{Co}_{16} \text{ \AA} / \text{Mn}_{4.8} \text{ \AA}]_{30}$ superlattice performed at the LURE synchrotron reveals two strong satellite peaks, which confirm the abrupt contrast of composition at the interfaces. The quantitative analysis of these spectra are in progress.

Now we discuss the variation of the average lattice spacing D . In Fig. 5, $1/D$ is plotted as a function of the relative cobalt concentration for the $[\text{Co}_{24} \text{ \AA} / \text{Mn}_{t_{\text{Mn}}}]_{12}$ series. Some information can be obtained from analyzing this curve. D can be written

$$D = \frac{n_{\text{Co}} \times d_{\text{Co}} + n_{\text{Mn}} \times d_{\text{Mn}}}{n_{\text{Co}} + n_{\text{Mn}}}, \quad (1)$$

where n_{Co} and n_{Mn} are, respectively, the number of Co and Mn monolayers in each layer and d_{Co} and d_{Mn} correspond to their respective lattice spacings. Equation (1) leads to the expression

$$\frac{1}{D} = \left[\frac{t_{\text{Co}}}{t_{\text{Co}} + t_{\text{Mn}}} \right] \left[\frac{1}{d_{\text{Co}}} - \frac{1}{d_{\text{Mn}}} \right] + \frac{1}{d_{\text{Mn}}}, \quad (2)$$

where $t_i = n_i \times d_i$ is the thickness of the i sublayer. The first term in parentheses is equal to the relative concentration of cobalt c_{Co} .

If we make the rough assumption that the interfaces between Co and Mn are incoherent and that there are neither interdiffusion nor roughness, d_{Co} and d_{Mn} are constants in each sublayer and can be deduced from the

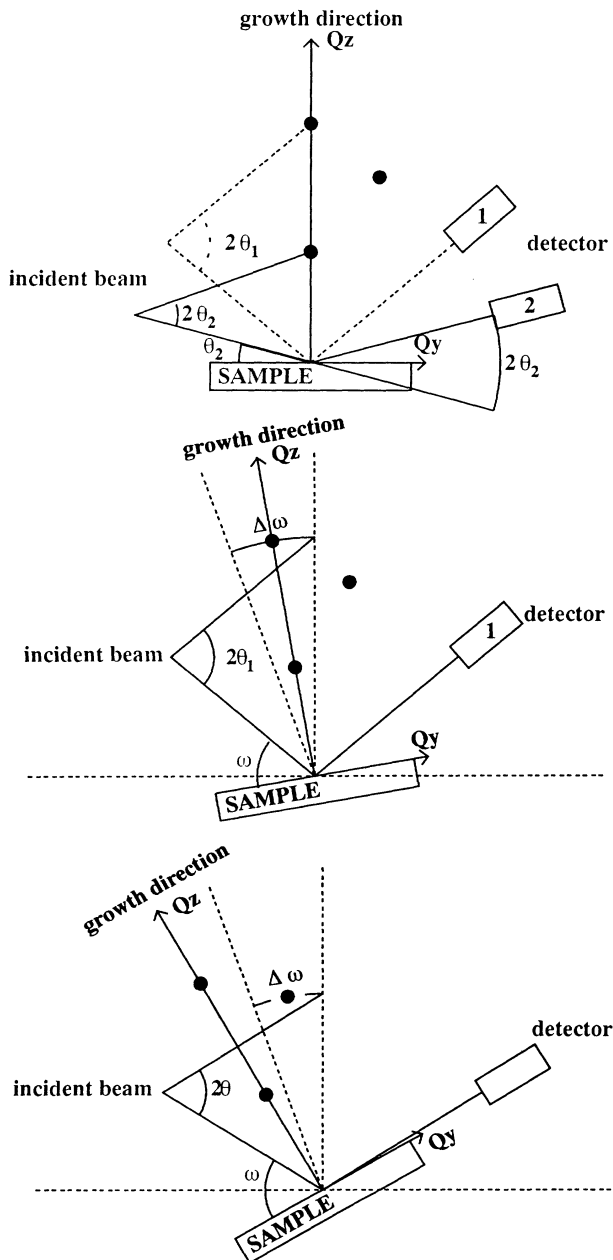


FIG. 3. Ewald construction showing how the reciprocal space is scanned in the three different x-ray diffractometer geometries. The black dots represent the reciprocal lattice points. ω is the angle between the incident beam direction and the film plane. θ is half the angle between the incident beam direction and the direction joining the goniometer center to the detector. (a) $\theta/2\theta$ scans: $I(0,0,Q_z)$ is collected; $\omega = \theta$. (b) Rocking curves in symmetric geometry: $I(0,Q_y,Q_z = \text{const})$ is collected; ω varies around a fixed θ . (c) Rocking curves in asymmetric geometry: $I(Q_x,Q_y,Q_z)$ is collected; for fixed values of θ , ω is varied to scan a range of the reciprocal space.

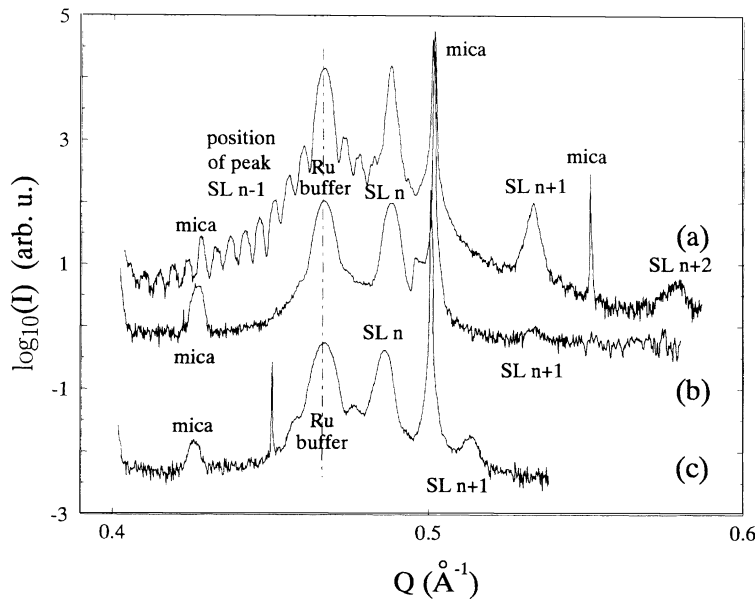


FIG. 4. $\theta/2\theta$ scans showing the superlattice peaks in addition to the buffer and mica peaks. The superlattices and wavelengths are the following: (a) $[\text{Co}_{16}\text{\AA}/\text{Mn}_{4.8}\text{\AA}]_{30}$, $\lambda=1.8975\text{\AA}$; (b) $[\text{Co}_{16}\text{\AA}/\text{Mn}_{4.8}\text{\AA}]_{12}$, $\lambda=1.5406\text{\AA}$; and (c) $[\text{Co}_{24}\text{\AA}/\text{Mn}_{12.8}\text{\AA}]_{12}$, $\lambda=1.5406\text{\AA}$.

plot of $1/D$ as the extrapolations at c_{Co} equal to 1 and 0.

The best fit of the experimental data shown in Fig. 5 leads to two straight lines crossing at a c_{Co} value corresponding to a Mn thickness of about 12 Å. This is the Mn thickness where the superstructure of the Mn sublayer appears on the RHEED patterns and confirms the structural change in the Mn layers.

The extrapolations to pure elements give different lattice spacings for the Co and Mn sublayers for the two straight lines. For $t_{\text{Mn}} < 12\text{\AA}$, the extrapolated values are $d_{\text{Co}}=2.038\pm 0.001\text{\AA}$ and $d_{\text{Mn}}=2.088\pm 0.003\text{\AA}$, while for $t_{\text{Mn}} > 12\text{\AA}$ they are $d_{\text{Co}}=2.027\pm 0.006\text{\AA}$ and $d_{\text{Mn}}=2.116\pm 0.009\text{\AA}$.

In bulk Co the stable phase at room temperature is hcp and undergoes a martensitic phase transition to a fcc structure around 400°C.²² The corresponding distances between compact planes are $d_{\text{hcp}}(0002)=2.035\text{\AA}$ and $d_{\text{fcc}}(111)=2.047\text{\AA}$ at 300 K. The decrease of the cobalt spacing for Mn thicknesses equal to 12 Å suggests a structural change from fcc to hcp in the cobalt sublayers at $t_{\text{cr}}=12\text{\AA}$. The fcc cobalt phase is so stabilized by thin Mn interlayers ($t_{\text{Mn}} < t_{\text{cr}}$). This structure change within the cobalt layers will be clearly shown in the following by investigating the accessible reflections of the cobalt.

Moreover, the extrapolated d_{Mn} values show that the Mn structure for $t_{\text{Mn}} < t_{\text{cr}}$ is more compact along the growth direction than for larger t_{Mn} .

We show in Fig. 6 the coherence length L_{\perp} versus the Mn thickness for the $[\text{Co}_{24}\text{\AA}/\text{Mn}_{t_{\text{Mn}}}]_{12}$ series. This figure shows an abrupt change around t_{cr} . For $t_{\text{Mn}} < t_{\text{cr}}$, the coherence length increases with the Mn thickness and is about 80% of the whole superlattice thickness. Above t_{cr} the coherence length continuously decreases to attain 30% of the superlattice thickness for $t_{\text{Mn}}=32\text{\AA}$. A possible explanation of this behavior is a loss of coherence between both sublattices. This can be related to the fact that Mn adopts a different and complicated structure,²¹ while the cobalt remains compact.

B. Rocking curves

The rocking curves across the out-of-plane superlattice main Bragg peaks SL_n correspond to circular arcs, symmetric across the Q_z reciprocal line [Fig. 3(b)] and give information on the in-plane crystalline quality, such as the lateral coherence length (L_{\parallel}) of the atomic layers as well as the mosaic distribution of the epitaxial film. From the fits of the data points to a Gaussian shape, we obtain full widths at half maximum (W_{\parallel}) between 1.2° and 1.7°, depending on the sample, and with no evident correlation with the Mn thickness. This result implies the following remarks.

(1) Since the rocking curves of the Ru buffer layers have a FWHM around 1.3°, we do not observe a degradation of the in-plane crystal quality in the superlattices. Compared to other results of Co-based multilayers grown on mica substrates²³ (FWHM > 2°), we can consider that the in-plane quality of these Co/Mn superlattices is very satisfactory. To improve it, it would be essential to use

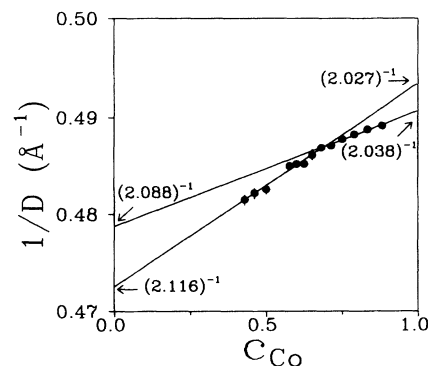


FIG. 5. Change of behavior observed when plotting the inverse of the average lattice spacing as a function of the relative concentration of cobalt, c_{Co} .

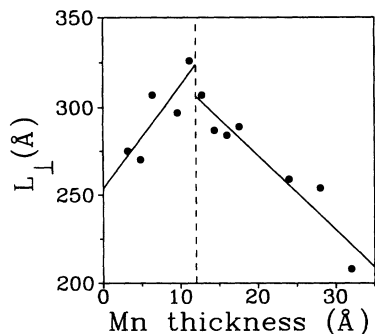


FIG. 6. Change of behavior observed when plotting the perpendicular coherence length L_{\perp} vs Mn thickness (the resolution of the instrument has been taken into account).

flat substrates such as sapphires and maybe other buffer layers such as Nb or Pt in which very narrow rocking curves can be obtained [FWHM $< 0.08^{\circ}$ for Nb (Refs. 24 and 25) and $< 0.5^{\circ}$ for Pt (Ref. 26)].

(2) W_{\parallel} does not show any change in the $[\text{Co}_{24 \text{ \AA}}/\text{Mn}_{t_{\text{Mn}}}]_{12}$ series with the Mn thickness even for $t_{\text{Mn}} > t_{\text{cr}}$. This is the sign that the in-plane crystalline quality is not affected by the phase change occurring in the Mn sublayers which requires another in-plane arrangement of the atoms.

(3) Neglecting any mosaicity in the sample, the rocking curves of the superlattices would give an in-plane coherence length between 30 and 40 Å. This value is very small and seems pessimistic. Transmission electron microscopy (TEM) observations²⁷ on similar buffer layers have shown that L_{\parallel} is much larger and would suggest that the large value of W_{\parallel} is predominantly due to misorientations of the growth axis. Obviously, the better method to determine the in-plane particle size is to measure the radial width of the in-plane (or nearly in-plane) peak. However, this experiment was not possible using our diffractometer as shown in Fig. 7.

C. Structures within the layers

From the $\theta/2\theta$ x-ray results, we have got some indications on a Mn phase change involving a modification of

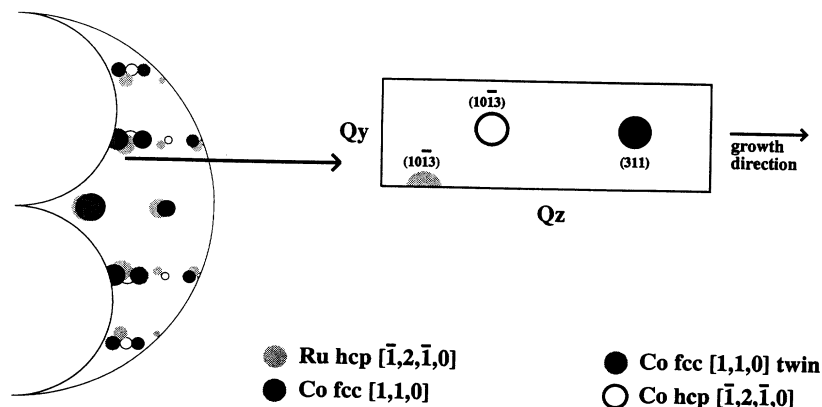


FIG. 7. Reciprocal-space region that can be attained in reflection geometry with Cu radiation and an exploded view of the region we have chosen to scan.

the stacking in the cobalt layers from fcc to hcp. In order to study the structure within the layers, we performed scans at reciprocal points with both nonzero out-of-plane Q_z and in-plane Q_y components [Fig. 3(c)].

The RHEED (Ref. 21) and TEM (Ref. 27) analyses have shown that for $t_{\text{Mn}} > t_{\text{cr}}$, the Mn layers consist of small grains with different structures (fcc and MgCu_2) and a large number of defects. Moreover, the interaction of matter with x rays is much smaller than that with electrons. All these points impede a study of the Mn structure by the x-ray technique. Indeed, up to now, no accessible reflections of the Mn structure were observed using x-ray experiments.

In order to distinguish between the two possible stackings of cobalt (hcp and fcc), we scanned the most dense reciprocal plane perpendicular to the film plane [indexed $(110)_{\text{fcc}}$ or $(\bar{1}\bar{2}10)_{\text{hcp}}$]. Our experimental conditions restrict the reflections that can be attained as shown in Fig. 7. Among these reflections, we scanned the region where the more intense reflections of Co [$(10\bar{1}3)_{\text{hcp}}$ and $(311)_{\text{fcc}}$] take place. The $(10\bar{1}3)$ intense reflection related to the Ru buffer layer is also included in this range (zoom in Fig. 7). We carried out the experiments for two samples below t_{cr} , $[\text{Co}_{24 \text{ \AA}}/\text{Mn}_{3.2 \text{ \AA}}]_{12}$ and $[\text{Co}_{24 \text{ \AA}}/\text{Mn}_{6.4 \text{ \AA}}]_{12}$, and one sample above t_{cr} , $[\text{Co}_{24 \text{ \AA}}/\text{Mn}_{24 \text{ \AA}}]_{12}$. In Fig. 8 we show the data corresponding to the three samples. For the three samples, the strong Ru $(10\bar{1}3)$ reflection is always the most intense one. This is due (a) to the fact that the sum of the thicknesses of the Ru buffer and capping layers is similar to the Co/Mn superlattice total thickness and (b) to the atomic number of Ru, which is higher than the Co and Mn ones.

(i) The $[\text{Co}_{24 \text{ \AA}}/\text{Mn}_{3.2 \text{ \AA}}]_{12}$ superlattice (S1) shows a $(311)_{\text{fcc}}$ peak without any contribution of the $(10\bar{1}3)_{\text{hcp}}$ peak, indicating that the Co layers are pure fcc [Fig. 8(a), left]. The presence of a weak diffuse line along the growth direction Q_z suggests the existence of a small number of stacking faults. We have also detected the presence of a $(311)_{\text{fcc}}$ twin peak related to a 180° twin (Fig. 7). Then this fcc structure presents two twin variants corresponding to the $(ABCABC\dots)$ and $(ACBACB\dots)$ stackings. From the widths of the (311) peak along Q_z , we estimate the coherence length of the stacking sequence ($L_{\text{fcc}\perp}$) to 40 Å [Fig. 8(a); right]. Despite the presence of twin variants, this coherence

length is much larger than the thickness of a single bilayer (around 27 Å), showing the presence of fully coherent Co and Mn sublattices with the same lattice parameters.

(ii) The $[\text{Co}_{24\text{ Å}}/\text{Mn}_{6.4\text{ Å}}]_{12}$ superlattice (S2) scan shows a very weak and broad $(311)_{\text{fcc}}$ peak with a more intense diffuse line along Q_z than for the S1 sample [Fig. 8(b), left]. The cobalt layers remain predominantly fcc with a higher density of stacking faults. The coherence length of the stacking sequence L_{fcc} is estimated to be at most 20 Å, which is thinner than one single cobalt layer [Fig. 8(b), right].

(iii) The $[\text{Co}_{24\text{ Å}}/\text{Mn}_{24\text{ Å}}]_{12}$ superlattice (S3) scan shows a very weak and broad $(10\bar{1}3)$ hcp peak with an intense diffuse line along Q_z [Fig. 8(c)]. The cobalt layers are now predominantly hcp with a high density of stacking faults. On this sample, we could not determine the coherence length of the stacking sequence (L_{hcp}) because of the proximity of the broad and intense $(10\bar{1}3)$ Ru hcp peak.

These data can be analyzed as follows: the three samples present equal cobalt but varying Mn thicknesses. The cobalt layers are thick (24 Å) and fully relaxed to the bulk lattice parameter as shown in Fig. 2. The RHEED analysis has shown that the growth of the free Mn surface is epitaxial but incoherent on the Co layer with an in-plane lattice parameter difference of about 10%. This result is in disagreement with the x-ray-diffraction experiment observations on very thin Mn layers (results on S1). The asymmetry between the growth of Mn on Co and that of Co on Mn and the difference between a free surface and a covered layer can explain this behavior. Indeed, the first stage of Co growth on Mn (about 5 monolayers) is semicoherent. The energy needed for the wetting of a Co surface on Mn is the sum of the surface free energy of the Co monolayer, $E_{\text{Co}}^{\text{surf}}$, the interface free energy between Mn and Co, $E_{\text{Co/Mn}}$, and the elastic energy $E_{\text{Co}}^{\text{el}}$ if the surface is strained by the substrate.²⁸ In the case of Mn on Co, there is no elastic energy contribution since the growth of Mn on Co is incoherent. When the

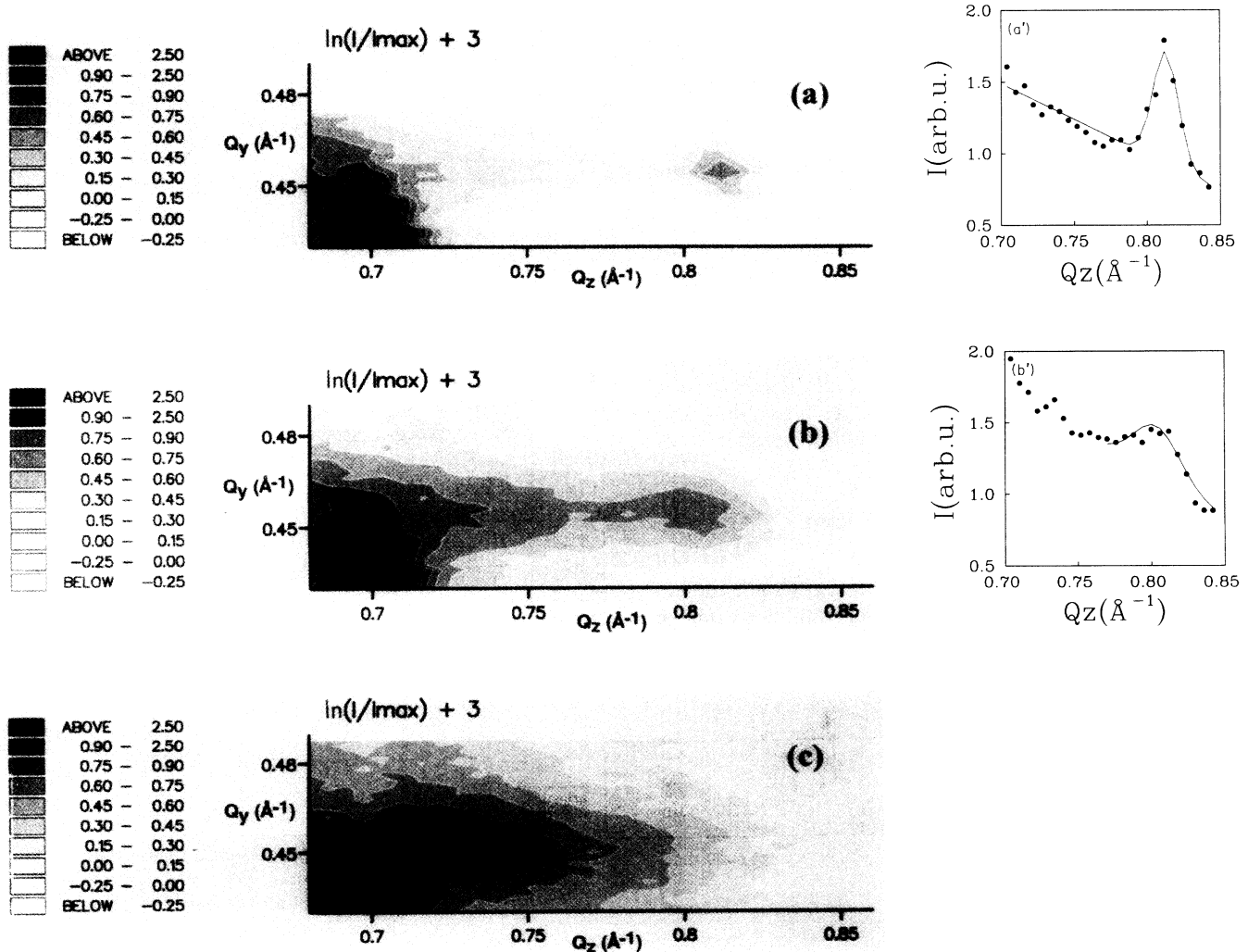


FIG. 8. On the left: diffraction from the different samples (a) S1, $[\text{Co}_{24\text{ Å}}/\text{Mn}_{3.2\text{ Å}}]_{12}$; (b) S2, $[\text{Co}_{24\text{ Å}}/\text{Mn}_{6.4\text{ Å}}]_{12}$; and (c) S3, $[\text{Co}_{24\text{ Å}}/\text{Mn}_{24\text{ Å}}]_{12}$. On the right: cross sections along Q_z through the $(311)_{\text{fcc}}$ Co peak for the two first samples.

cobalt layer is thick enough to reach the bulk lattice parameter, the elastic energy within the cobalt layer can be minimized by forming epitaxial dislocations at the interfaces and/or by constraining the Mn underlayer. The resulting structure depends on the energy needed for both processes, respectively, $E_{\text{Mn/Co}}^{\text{disl}}$ and $E_{\text{Mn}}^{\text{el}}$. The cost in energy of the contraction of the Mn underlayer is proportional to the Mn thickness $E_{\text{Mn}}^{\text{el}} = t_{\text{Mn}} \times \varepsilon_{\text{Mn}}^{\text{el}}$, and so there is a critical thickness, above which the creation of epitaxial dislocations is favored ($t_{\text{Mn}} > E_{\text{Mn/Co}}^{\text{disl}} / \varepsilon_{\text{Mn}}^{\text{el}}$). X-ray results have shown that for *S1* the relaxation of the cobalt top layer has induced elastic strains in the Mn underlayer which are sufficient to contract the Mn in-plane lattice parameter to the bulk cobalt value. This is not surprising as for such a thin layer all Mn atoms are located at the interfaces.

For the thicker Mn sublayers (*S2*, *S3*), where some Mn are in inner planes, we observe a loss of coherency between Mn and Co sublattices as a result of the presence of epitaxial dislocations, indicating that the elastic strains are no longer sufficient to contract the entire Mn layer. Moreover, in the case of *S3*, the coherence length normal to the film plane (L_{\perp}), deduced from the $\theta/2\theta$ scans, is smaller (5 bilayers) than in *S2* (10 bilayers), indicating that in *S3* the coherence is more rapidly lost as a result of a higher density of dislocations than in *S2*.

Before going further in the understanding of the phase change mechanism, we will present some complementary results obtained by ferromagnetic resonance.

V. FERROMAGNETIC RESONANCE RESULTS

The purpose of these experiments is to distinguish fcc and hcp components in the crystalline structure of the cobalt layers and to study their related structural defects on the $[\text{Co}_{24} \text{ \AA} / \text{Mn}_{t_{\text{Mn}}}]_{12}$ series. Ferromagnetic resonance (FMR) is a well-established method for a quantitative determination of magnetic anisotropies and inhomogeneities in magnetic superlattices.^{29–32} As hcp and fcc cobalt bulk structures display very different magnetocrystalline (MC) anisotropies, FMR turns out to be particularly useful to determine the crystallographic structure within the cobalt layers (fcc, hcp, or in between) and the density of stacking faults.

A. Ferromagnetic resonance measurements

FMR was measured at 9.8 GHz and at room temperature (RT) in a TE_{011} cavity that allowed us to vary the angle θ_H of the applied field with respect to the film normal. The FMR data were analyzed using the standard theory which involves solving the Landau-Lifshitz equation of motion for the magnetization \mathbf{M} in presence of an external applied field \mathbf{H}_{ext} , an uniaxial effective anisotropy field $H_{K_{\text{eff}}}$ and a microwave driving field.^{1,30,31}

The in-plane magnetization curves measured at RT using an alternating gradient force magnetometer of all the Co/Mn samples are fully saturated for a field of about 100 Oe, which indicates that adjacent cobalt layers are not antiparallel coupled. In this case, the calculation of the FMR dispersion relation for this system can be

simplified by the standard single-layer model.^{30,31}

The contribution to the energy density due to the anisotropy is given by

$$E_K = \left[2\pi M^2 + K_{\text{MC}} + 2 \frac{K_s}{t_{\text{Co}}} \right] \cos^2 \theta,$$

where θ is the angle between \mathbf{M} and the surface normal, $2\pi M^2$ corresponds to the demagnetizing energy density, K_{MC} to the magnetocrystalline anisotropy which reflects the symmetry of the crystal, and $2K_s/t_{\text{Co}}$ the anisotropy coming from the two interfaces for each Co layer. Here we have neglected (i) the magnetoelastic anisotropy, which is small, since the cobalt layers are fully relaxed as deduced from RHEED and x-ray results (Sec. III and IV), and (ii) the small six-order in-plane anisotropy present in these samples.³³ The equilibrium and resonance conditions for the magnetization can be found in Refs. 29–32. One gets simple expressions in the two particular geometries: H_{ext} along ($\theta_H = 0^\circ$) and perpendicular ($\theta_H = 90^\circ$) to the film plane which allow one to obtain a direct determination of the effective anisotropy field $H_{\text{eff}} = 2K_{\text{eff}}/M_s$.

We have determined the MC anisotropy of the cobalt layers for each of the $[\text{Co}_{24} \text{ \AA} / \text{Mn}_{t_{\text{Mn}}}]_{12}$ samples by deducing independently the following.

(i) The demagnetizing field from direct magnetization measurements. The saturation magnetizations for all samples of the $[\text{Co}_{24} \text{ \AA} / \text{Mn}_{t_{\text{Mn}}}]_{12}$ series are found to be very close (about 16 kOe) with a slight dispersion of about 5% within the experimental error bars because of uncertainties in the area and fluctuation in the thickness of the samples.³³

(ii) The interfacial magnetic anisotropy from FMR measurements on three $[\text{Co}_{t_{\text{Co}}} / \text{Mn}_{t_{\text{Mn}}}]_2$ series with constant Mn layer thicknesses ($t_{\text{Mn}} = 4, 10, \text{ and } 15 \text{ \AA}$) and varying Co layer thicknesses, using the procedure described in Refs. 33 and 34. We found $2K_s \simeq 1 \text{ erg/cm}^2$, which does not vary with the Mn thickness.³³

B. Results and analysis

Figure 9 is a plot of the magnetocrystalline anisotropy field H_{MC} versus t_{Mn} for the $[\text{Co}_{24} \text{ \AA} / \text{Mn}_{t_{\text{Mn}}}]_{12}$ series. The field is directly related to the anisotropy constant using the relation $H_{\text{MC}} = 2K_{\text{MC}}/M_s$. The strong variation of H_{MC} with Mn thickness can be interpreted in the following way.

For the perfect hcp and fcc structures with the same saturation magnetization as the studied series ($4\pi M_s = 16 \text{ kOe}$), the magnetocrystalline anisotropy field should be $H_{\text{MC}}^{\text{hcp}} \simeq 6.7 \text{ kOe}$ and $H_{\text{MC}}^{\text{fcc}} \simeq 0.35 \text{ kOe}$, respectively, as deduced from Co bulk anisotropy constants.³⁵ First, for the $[\text{Co}_{24} \text{ \AA} / \text{Mn}_{3.2 \text{ \AA}}]_{12}$ superlattice (sample *S1*), the very low value of H_{MC} (0.5 kOe) close to $H_{\text{MC}}^{\text{fcc}}$ confirms the almost perfect fcc structure of the cobalt layers observed by x rays. Then, for samples with intermediate Mn thicknesses $3.2 < t_{\text{Mn}} < 12 \text{ \AA}$, the anisotropy field reaches a plateau with $H_{\text{MC}} = 1.6 \pm 0.3 \text{ kOe}$ and closer to $H_{\text{MC}}^{\text{fcc}}$ than to $H_{\text{MC}}^{\text{hcp}}$. This result suggests that the structure of

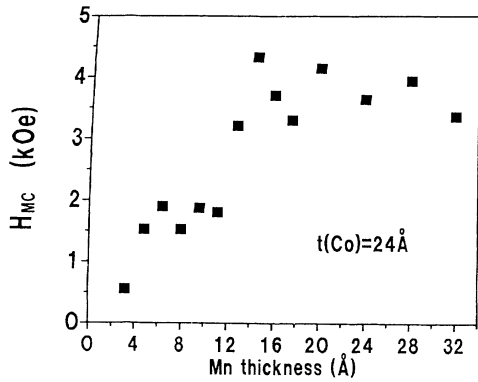


FIG. 9. Magnetocrystalline anisotropy field H_{MC} as a function of Mn thickness for the $[\text{Co}_{24 \text{ \AA}}/\text{Mn}_{t_{\text{Mn}}}]_{12}$ series. H_{MC} has been determined from the effective anisotropy field H_{eff} measured by FMR.

the cobalt layers is predominantly fcc in this Mn thickness range with no indication of an increased hcp Co proportion. Finally, for samples with $t_{\text{Mn}} > 12 \text{ \AA}$, the magnetocrystalline anisotropy field increases with a large spread of values. This indicates that in these samples the Co layers have a predominant hcp structure, but with some inclusions of the fcc Co phase.

In order to determine the structural quality of the samples in terms of the perfection of the fcc or hcp phase, we studied the field linewidth of the absorption peaks in both perpendicular ($\theta_H = 90^\circ$) and parallel ($\theta_H = 0^\circ$) orientations of the external applied field with respect to the film plane. In the Co/Mn superlattices, the resonance linewidth ΔH originates from two sources besides the intrinsic damping mechanism. The first contribution is the distribution of the directions of the c axis for different crystallites. The other one is the internal effective field inhomogeneity which arises from the presence of both fcc and hcp phases within the cobalt layers. The resonance linewidth (denoted, respectively, ΔH_\perp and ΔH_\parallel for θ_H equal to 0° and 90°) are plotted in Fig. 10 as a function of t_{Mn} for the $[\text{Co}_{24 \text{ \AA}}/\text{Mn}_{t_{\text{Mn}}}]_{12}$ superlattices. The results

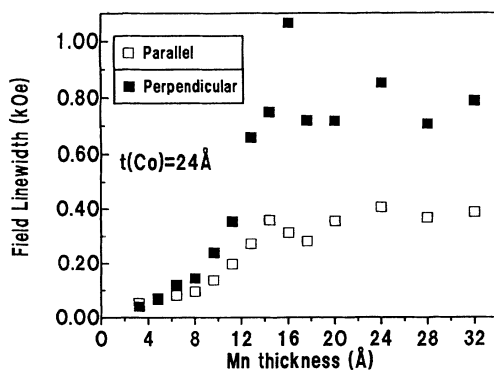


FIG. 10. Linewidths of the resonance field ΔH in perpendicular (solid square) and parallel (open square) orientations of the external field, as a function of Mn thickness for the $[\text{Co}_{24 \text{ \AA}}/\text{Mn}_{t_{\text{Mn}}}]_{12}$ series.

are complementary to the previous observations concerning the absolute value of the effective anisotropy fields and allow one to make the following remarks: (i) For the $[\text{Co}_{24 \text{ \AA}}/\text{Mn}_{3.2 \text{ \AA}}]_{12}$ sample, the small values of ΔH_\parallel (48 Oe) and ΔH_\perp (38 Oe) at 9.8 GHz show that there are only a very small number of defects. In fact, this sample compares favorably with the narrowest lines observed in ultrathin films and superlattices.^{36,37} This result is compelling evidence that our sample possesses a very good structure. It is in agreement with the RHEED and x-ray results which have shown the high crystalline quality of the whole $[\text{Co}_{24 \text{ \AA}}/\text{Mn}_{t_{\text{Mn}}}]_{12}$ series. This indicates that the spatial fluctuations of the c axis ($\approx 1.5^\circ$ as measured by x-ray diffraction) do not affect particularly the field linewidth and implies that its contribution for the whole series of samples should be negligible. Moreover, the spread of the internal fields due to the presence of hcp grains is very small and confirms the high purity of the fcc phase in this particular sample. (ii) For samples with thicker Mn thicknesses ($t_{\text{Mn}} > 6 \text{ \AA}$) the field linewidth increases with t_{Mn} , becoming anisotropic and larger along the perpendicular direction. This can be understood if the main contribution to the FMR absorption linewidth is due to the inhomogeneous line broadening as was suggested by Chappert *et al.*³⁰ Their idea is that the specimen can be considered as a collection of independent domains: Each region is supposed to be subject to a different anisotropy field due to presence of stacking faults or grains having different structures and therefore has a different resonance field. Indeed, the FMR fields of perfect hcp and fcc grains for which $4\pi M_s = 16 \text{ kOe}$ and $K_s = 0.5 \text{ erg/cm}^2$ are similar to that of the $[\text{Co}_{24 \text{ \AA}}/\text{Mn}_{t_{\text{Mn}}}]_{12}$ samples are, respectively, $H_\parallel^{\text{fcc}} \approx 0.75 \text{ kOe}$, $H_\parallel^{\text{hcp}} \approx 1.4 \text{ kOe}$ for $\theta_H = 0^\circ$ and $H_\perp^{\text{fcc}} \approx 14 \text{ kOe}$, $H_\perp^{\text{hcp}} \approx 7.9 \text{ kOe}$ for $\theta_H = 90^\circ$. The internal field distribution broadens the absorption line at all angles, but the maximum broadening occurs when the field is applied perpendicularly to the film plane. Indeed, for $\theta_H = 90^\circ$, the difference between the hcp and fcc FMR fields is the largest ($H_\perp^{\text{fcc}} - H_\perp^{\text{hcp}} \approx 6 \text{ kOe}$) and the perpendicular resonance linewidth provides a measure of the anisotropy field distribution. Consequently, ΔH_\perp gives an indication of the partition of the hcp and fcc phases within the cobalt sublayers. However, for $\theta_H = 0^\circ$, the FMR field is much less sensitive to the variations of the anisotropy fields ($H_\parallel^{\text{fcc}} - H_\parallel^{\text{hcp}} \approx 0.6 \text{ kOe}$), inducing a smaller field linewidth. Farle *et al.*³³ have reported a fit of the field linewidth for the $[\text{Co}_{24 \text{ \AA}}/\text{Mn}_{t_{\text{Mn}}}]_{12}$ series, assuming that the anisotropy is distributed around its mean value (defined in Fig. 9) according to a Gaussian distribution. They have shown that a fluctuation smaller than $\pm 2\%$ in the magnetocrystalline anisotropy is sufficient to explain both line broadenings (ΔH_\perp and ΔH_\parallel) for samples with Mn thickness $t_{\text{Mn}} < 12 \text{ \AA}$. Such a variation can be attributed to the small density of stacking faults which strongly affect the MC anisotropy. In predominantly fcc Co, it is clear that a stacking fault such as $ABCABABC\dots$ would strongly affect two adjacent atomic layers where the involved atoms are in a hcp

nearest-neighbor environment. In the presence of such stacking faults in the cobalt sublayers, the average value of H_{MC} is expected to decrease and the linewidth to broaden. However, for thicker Mn thicknesses, for which the Co sublayers have now a predominant hcp structure ($t_{Mn} > 12 \text{ \AA}$), the sudden jump in ΔH_L up to about 0.8 kOe (Fig. 10) indicates a larger spread of the internal field than in the previous case (corresponding to $\pm 8\%$ fluctuations in the MC anisotropy³³), which is considerable if compared to other very clean hcp cobalt structures (for example, Co/Ru superlattices³⁸ prepared in the same conditions which have parallel and perpendicular linewidths of about 0.2 kOe). This is related to a large increase of the number of stacking faults, which tend to increase the cubic environment of the cobalt atoms within the Co sublayers. Most striking is the fact that the field linewidth does not change for larger Mn thicknesses up to $t_{Mn} \approx 32 \text{ \AA}$, as shown in Fig. 10, suggesting that the number of stacking faults remains approximately the same.

VI. DISCUSSION

The results described in this paper show that a phase change takes place within both Mn and Co layers at a critical Mn thickness of 12 \AA . In the following, we discuss possible explanations for the structural change in both Mn thickness ranges.

A. Thin Mn layers

Up to 6 Mn monolayers, the Mn layers being highly strained, Co and Mn are stabilized in out-of-equilibrium close-packed structures (fcc stacking). Such a metastable fcc Co structure has been already observed in the case of the epitaxial growth of cobalt on fcc templates [for example, (100) or (111) Cu (Refs. 25, 26, 32, and 39) or Ni (Ref. 7)]. The fcc structure of cobalt is stabilized when deposited on thin Mn layers (Sec. IV). This indicates that these close-packed layers act like a fcc template even for only 2 monolayers of Mn, where the stacking sequence is not yet completely defined within the Mn layers. Noting, moreover, that the only close-packed Mn phase stable in the bulk is the fcc γ -Mn and that fcc Mn grains have been observed by RHEED for thicker Mn layers (Sec. III and Ref. 21), we think that Mn has a cubic symmetry even if experimentally we did not determine the stacking, which is very difficult for so thin layers. The stabilization of a metastable structure, such as the fcc cobalt at room temperature, arises through chemical and elastic interactions between Co and substrate atoms.

1. Elastic interactions

We have seen in Sec. III that the Co in-plane parameter returns to the Co bulk value within 7 monolayers in the case of thin Mn layers where fcc Co is observed. Moreover, by x-ray diffraction, we have measured a fcc lattice parameter corresponding to bulk fcc Co within the error bars. Thus Co appears to keep the fcc structure even when the residual stresses within the Co layers are very small. The elastic energy is thus not the predom-

inant term of the total energy in the case of the stabilization of the fcc Co phase by a fcc Mn substrate. We can draw a parallel with the case of Co/Ru multilayers, where the misfit between the two in-plane parameters is equivalent (10%) and does not induce either a phase change or even any stacking faults in the Co hcp phase.⁴⁰

2. Chemical interactions

The deposition of an overlayer onto a close-packed (111) fcc surface involves two types of sites in equal numbers: the normal sites, which, when occupied, continue the fcc stacking, and the fault sites, which give rise to a stacking fault. The binding energies on the two types of sites depend on the nature of the adatom. Indeed, recent experiments⁴¹ have confirmed that the atomic position adopted by an adatom is strongly determined by its chemical identity. Our observations show that the chemical interactions between Co and Mn minimize the total energy when the Co is bound on normal sites. Moreover, the fcc stacking in Co is favored by the presence of Mn atoms even at long distances. Indeed, we observe through x-ray diffraction on these superlattices that the fcc stacking is conserved in 24- \AA -thick Co layers in between two thin Mn layers. The extension of the interactions responsible for the structural change is thus at least 12 \AA (about 5 monolayers). One may speculate that this occurs via chemically initiated charge transfers. All these points can be compared to the effect of Mn impurities in bulk cobalt:⁴² The martensitic transformation temperature decreases abruptly with the Mn concentration to reach room temperature at about 25 at. %, showing that Mn stabilizes the fcc phase of Co.

B. Thick Mn layers

As the thickness of the Mn layers is increased, there is a trade-off between reduced strains in the Mn and a higher density of epitaxial dislocations, leading to a lower coherence between the Mn and Co layers. Eventually, for a Mn layer thickness of 6 monolayers, the dislocation density at the interfaces is maximum with very little strains in either layer. This increase of the dislocation density is matched by an increase of the occurrence of Co fcc stacking faults. In fact, the cobalt essentially reverts to its normal bulk hcp structure by virtue of this high incidence of stacking faults. In parallel, manganese also tends to approach its bulk structure. Indeed, it adopts a MgCu_2 -type structure, based on a building block existing in the Mn- α structure, stable at room temperature in the bulk. This structure change is progressive (some fcc grains can still be observed through RHEED) and incomplete (the bulk stable phase is not attained). Remarkably, the stacking fault density in this new Co hcp phase is considerable (Sec. V) and remains relatively constant when the Mn layer thickness changes. The Co hcp stacking fault density is significantly higher than expected for unstrained Co films. For example, in Co/Ru superlattices, Co has a very clean hcp structure with a small stacking fault density.⁴⁰ We think that the high stacking fault density observed in these unstrained Co/Mn samples relates to the chemical interactions between Co and

Mn. These interactions would then favor the fcc Co stacking even when the Mn structure is no longer close packed.

VII. CONCLUSION

Until now, the origins of metastable phases induced by epitaxy have remained unclear. Different contributions determine the free energy of these metastable structures, but their relative importance has never been resolved to our knowledge. This paper gives an indication of the relative importance of chemical and elastic strain energies in Co/Mn superlattices. To stabilize the metastable fcc cobalt phase, both energy terms are required, but the chemical interactions alone are sufficient to induce a faulted Co hcp structure. This indicates that chemical energy existence can favor a certain type of stacking se-

quence even if the latter does not correspond to the template structure. It highlights the importance of considering carefully the chemistry of the constituent metals when attempting to engineer a particular superlattice structure.

ACKNOWLEDGMENTS

The authors gratefully acknowledge M. Bessière, S. Lefebvre, and H. Fisher for measurements of the anomalous x-ray diffraction on the LURE synchrotron. They also want to thank Dr. J. F. Gregg, Dr. M. Farle, Dr. P. Panissod, and Dr. G. Suran for very fruitful conversations, and G. Mathis and M. Acosta for technical assistance. This work was supported in part by the European Community Science Project ESPRIT3 Basic Research, "Study of Magnetic Multilayers for Magnetoresistive Sensors" (SmMmS).

- ¹B. Heinrich, S. T. Purcell, J. R. Dutcher, K. B. Urquhart, J. F. Cochran, and A. S. Arrott, *Phys. Rev. B* **38**, 12 879 (1988).
- ²G. A. Prinz, *Phys. Rev. Lett.* **54**, 1031 (1985).
- ³M. Maurer, J. C. Ousset, M. F. Ravet, and M. Picuch, *Europhys. Lett.* **9**, 803 (1989).
- ⁴J. Kubler, *Solid State Commun.* **72**, 631 (1989).
- ⁵V. L. Moruzzi, *Phys. Rev. Lett.* **57**, 2211 (1986); V. L. Moruzzi, P. L. Marcus, and C. Pattnaik, *Phys. Rev. B* **37**, 8003 (1988).
- ⁶V. L. Moruzzi and P. M. Marcus, *Phys. Rev. B* **38**, 1613 (1988).
- ⁷G. H. O. Daalderop, P. J. Kelly, and F. J. A. den Broeder, *Phys. Rev. Lett.* **68**, 682 (1992).
- ⁸R. W. G. Wyckoff, *Crystal Structures* (Wiley, New York, 1963), pp. 50–52.
- ⁹J. L. Fry, Y. Z. Zhao, N. E. Brener, G. Fuster, and J. Callaway, *Phys. Rev. B* **36**, 868 (1987).
- ¹⁰G. Fuster, N. E. Brener, J. Callaway, J. L. Fry, Y. Z. Zhao, and D.A. Papaconstantopoulos, *Phys. Rev. B* **38**, 423 (1988).
- ¹¹B. Heinrich, A. S. Arrott, C. Liu, and S. T. Purcell, *J. Vac. Sci. Technol. A* **5**, 1935 (1988); A. S. Arrott, B. Heinrich, S. T. Purcell, J. F. Cochran, and K. B. Urquhart, *J. Appl. Phys.* **61**, 3721 (1988).
- ¹²D. Tian, H. Li, S. C. Wu, F. Jona, and P. M. Marcus, *Phys. Rev. B* **45**, 3749 (1992).
- ¹³G. A. Prinz, *Mater. Res. Soc. Bull.* **13**, 28 (1988).
- ¹⁴B. T. Jonker, J. J. Krebs, and G. A. Prinz, *Phys. Rev. B* **39**, 1399 (1989).
- ¹⁵D. Stoeffler, K. Ounadjela, J. Sticht, and F. Gautier (unpublished).
- ¹⁶The only exception concerns the growth of cobalt overlayer on the Mn seed layer in which no improvement of the RHEED patterns is observed. Indeed, the quality of the Ru buffer layer is not degraded by the deposit of a few atomic planes of the Mn seed layer.
- ¹⁷S. Pizzini, F. Baudelet, A. Fontaine, M. Galtier, D. Renard, and C. Marlière, *Phys. Rev. B* **47**, 8754 (1993).
- ¹⁸J. A. Bain, L. J. Chyung, S. Brennan, and B. M. Clemens, *Phys. Rev. B* **44**, 1184 (1991), and references therein.
- ¹⁹G. W. R. Leibrandt, R. van Wijk, and F. H. P. Habraken, *Phys. Rev. B* **47**, 6630 (1993).
- ²⁰E. Fullerton, J. Guimpel, O. Nakamura, and I. K. Schuller, *Phys. Rev. Lett.* **69**, 2859 (1992).
- ²¹Y. Henry, V. Pierron-Bohnes, P. Vennegues, and K. Ounadjela (unpublished).
- ²²W. B. Pearson, *Handbook of Lattice Spacings and Structures of Metals* (Pergamon, New York, 1958), Vol. 1, p. 501.
- ²³F. Hakkens, W. Coene, and F. J. A. Den Broeder, in *Magnetic Surfaces, Thin Films and Multilayers*, edited by S. S. P. Parkin, H. Hopster, J. P. Renard, T. Shinjo, and W. Zenn, MRS Symposia Proceedings No. 231 (Materials Research Society, Pittsburgh, 1992), p. 397; M. Picuch (private communication).
- ²⁴P. M. Reimer, H. Zabel, C. P. Flynn, and J. A. Dura, *Phys. Rev. B* **45**, 11 426 (1991).
- ²⁵P. Bödeker, A. Abromeit, K. Bröhl, P. Sonntag, N. Metoki, and H. Zabel, *Phys. Rev. B* **47**, 2353 (1993).
- ²⁶S. S. P. Parkin, R. F. Marks, R. F. C. Farrow, G. R. Harp, Q. H. Lam, and R. J. Savoy, *Phys. Rev. B* **46**, 9262 (1991).
- ²⁷A. Michel (private communication).
- ²⁸F. Gautier and D. Stoeffler, *Surf. Sci.* **249**, 265 (1991).
- ²⁹M. Farle, A. Berghaus, and K. Baberschke, *Phys. Rev. B* **39**, 4838 (1989).
- ³⁰C. Chappert, K. Le Dang, P. Beauvillain, H. Hurdequint, and D. Renard, *Phys. Rev. B* **34**, 3192 (1986).
- ³¹B. Heinrich, Z. Celinski, J. F. Cochran, A. S. Arrott, and K. Myrtle, *J. Appl. Phys.* **70**, 5769 (1991).
- ³²B. Heinrich, J. F. Cochran, M. Kowalewski, J. Kirshner, Z. Celinski, A. S. Arrott, and K. Myrtle, *Phys. Rev. B* **44**, 9348 (1991).
- ³³M. Farle, K. Ounadjela, and Y. Henry (unpublished); K. Ounadjela, Y. Henry, M. Farle, and P. Vennegues (unpublished).
- ³⁴B. N. Engel, C. D. England, R. A. van Leeuwen, M. H. Wiedemann, and C. M. Falco, *Phys. Rev. Lett.* **67**, 1910 (1991).
- ³⁵W. Sucksmith and J. E. Thompson, *Proc. R. Soc. London A* **255**, 362 (1954).
- ³⁶B. Heinrich and Z. Celinski, *J. Appl. Phys.* **70**, 5769 (1991).
- ³⁷G. A. Prinz, B. T. Jonker, J. J. Krebs, J. M. Ferrari, and F. Kovanic, *Appl. Phys. Lett.* **48**, 1756 (1986).
- ³⁸K. Ounadjela, D. Muller, A. Dinia, A. Arbaoui, G. Suran, and P. Panissod, *Phys. Rev. B* **45**, 7768 (1992).
- ³⁹F. J. Lamelas, C. H. Lee, H. He, W. Vavra, and R. Clarke, *Phys. Rev. B* **40**, 5837 (1989); F. J. A. Den Broeder, W. Hoving, and P. J. H. Bloemen, *J. Magn. Mater.* **93**, 562 (1991).

⁴⁰D. Muller, K. Ounadjela, P. Venegues, V. Pierron-Bohnes, A. Arbaoui, J. P. Jay, A. Dinia, and P. Panissod, *J. Magn. Mater.* **104**, 1873 (1992).

⁴¹S. C. Wang and G. Ehrlich, *Phys. Rev. Lett.* **68**, 1160 (1992);

B. Piveteau, D. Spanjaard, and M. C. Desjonquères, *Phys. Rev. B* **46**, 7121 (1992).

⁴²M. Acet, C. John, and E. F. Wassermann, *J. Appl. Phys.* **70**, 6556 (1991).

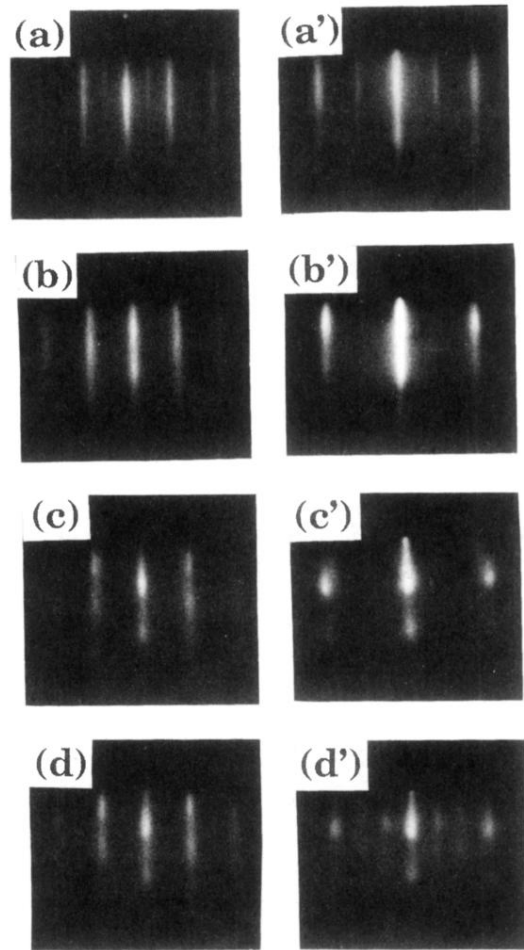


FIG. 1. RHEED patterns of $[\text{Co}_{24 \text{ \AA}}/\text{Mn}_{24 \text{ \AA}}]_{12}$ along the two characteristic azimuths [left $(\bar{1}\bar{2}10)$ and right $(10\bar{1}0)$] on (a),(a') Ru buffer, (b),(b') after 3 monolayers of Mn on the Ru buffer, (c),(c') after 3 monolayers of Mn on the first Co layer and (d),(d') after depositing the second Mn layer on top of the first Co layer.

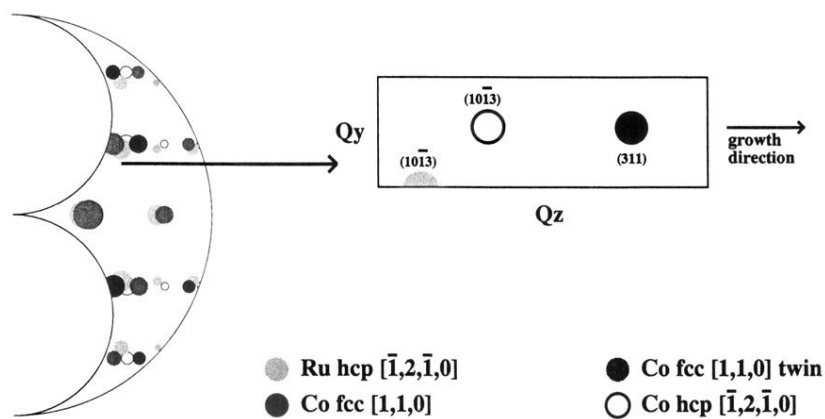


FIG. 7. Reciprocal-space region that can be attained in reflection geometry with Cu radiation and an exploded view of the region we have chosen to scan.

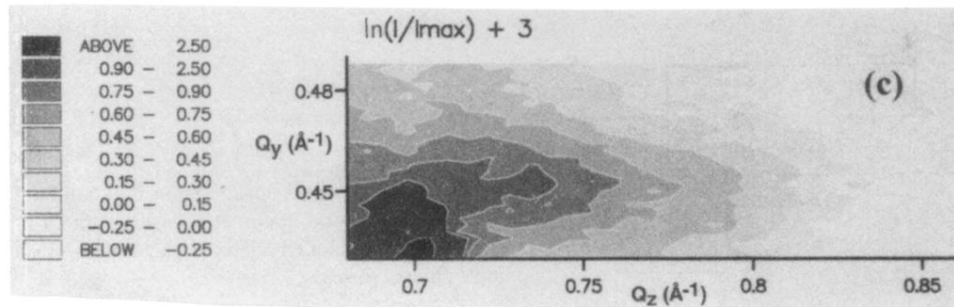
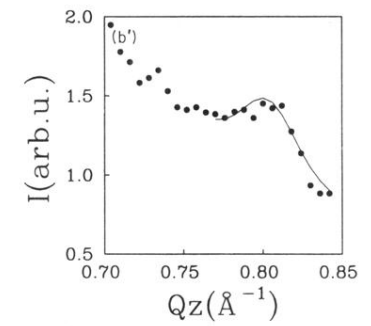
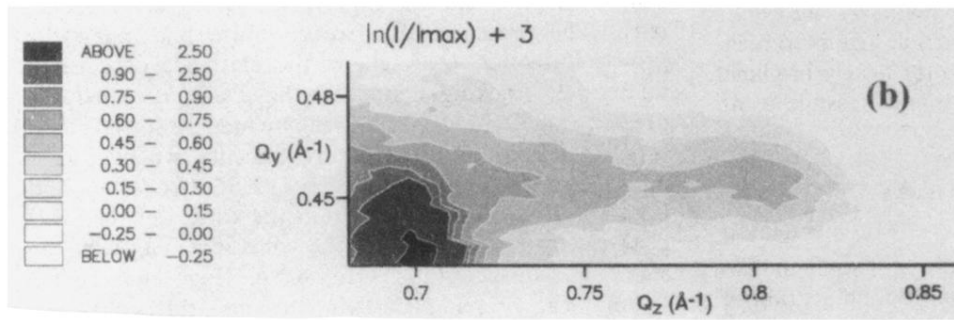
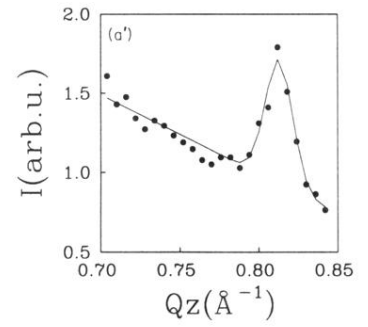
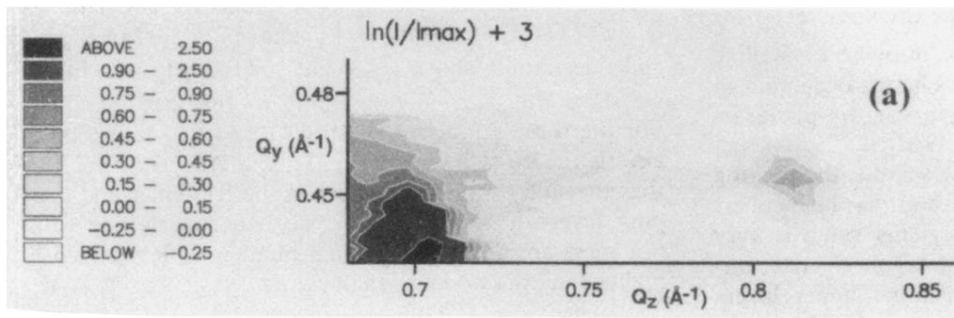


FIG. 8. On the left: diffraction from the different samples (a) $S1$, $[\text{Co}_{24} \text{Å} / \text{Mn}_{3.2} \text{Å}]_{12}$; (b) $S2$, $[\text{Co}_{24} \text{Å} / \text{Mn}_{6.4} \text{Å}]_{12}$; and (c) $S3$, $[\text{Co}_{24} \text{Å} / \text{Mn}_{24} \text{Å}]_{12}$. On the right: cross sections along Q_z through the $(311)_{\text{fcc}}$ Co peak for the two first samples.